



# Prominence of Narrow Groove on Pulsed Current GMA and SMA Welding of Thick Wall Austenitic Stainless Steel Pipe

Shrirang Kulkarni<sup>1</sup> · G. Rajamurugan<sup>2</sup>  · P. K. Ghosh<sup>3</sup>

Received: 25 February 2021 / Accepted: 10 May 2021 / Published online: 26 June 2021  
© The Indian Institute of Metals - IIM 2021

**Abstract** The pulsed current gas metal arc (PGMA) welding and shielded metal arc (SMA) welding with a narrow groove joint were used to weld the thick wall 304LN stainless steel pipe. The primary emphasis has been laid on the welding procedure by reducing the weld area with a narrow groove design. A constant heat input of  $7.5 \pm 0.5$  kJ/cm was used to perform the narrow gap SMA and PGMA welding of austenitic stainless steel pipe. The PGMA welding was carried out at two different  $\phi$  of 0.05 and 0.25 and groove width of 15 and 11 mm. The obtained results have shown that the narrow groove PGMA welds prepared at relatively lower  $\Omega$  having 4–7%  $\delta$ -ferrite content are comparatively less prone to solidification cracking than the SMA weld joint. The amount of porosity content was marginally increased in PGMA welds, whereas in the narrow groove SMA welds, the amount of porosity and inclusion content got increased by almost 30%. The narrow groove PGMA welds have significantly higher yield strength in both the longitudinal (363 MPa) and circumferential (466 MPa) directions than the SMA weld joints. Narrow groove PGMA welds have appreciably better Cv-impact toughness (126 J) and lateral expansion (2.5 mm) than that observed in SMA weld joint. The narrow groove PGMA weld (11 mm weld width) of various  $\phi$  of 0.05 and 0.25 show widespread ductile fracture behavior with fine dimples and significantly minor porosity content than the

SMA weld joints. The PGMA welds are comparatively less scattered in hardness across the weld and HAZ at both the  $\Omega$  and  $\phi$  levels.

**Keywords** Austenitic stainless steel · Narrow gap welding · V-groove · Inclusion content · PGMAW · SMAW

## 1 Introduction

Narrow groove welding has generated significant interest in the welding industry and has been the subject of much investigation in the last twenty years. But to date, there is some disagreement around a proper definition for the technique. Most of the authors have agreed that narrow gap welding is applied to any welding process used to join the heavy section ( $> 25$  mm). Virtually square butt joint with small gaps will yield a weld with low volume weld metal [1–3]. The advantages of narrow gap welding processes such as reducing welding time due to less weld deposition with the least number of beads reduce the severity of weld thermal cycle producing less axial and radial shrinkage. It may favorably affect the stresses at the root area compared to those observed in conventional groove welding. A low dwell time in the critical sensitizing temperature range due to less bead deposition and a favorable residual stress profile in the weld and heat-affected zone may improve the weld joint properties [3, 4].

However, to produce high-quality multi-pass narrow gap welds, one of the essential parameters, namely the width of the gap, must be maintained constant during the welding of each pass. With the reduction in gap width, access to the welding zone becomes more complex, and the welding process may be disrupted due to the short-circuiting of the

✉ G. Rajamurugan  
rajadmt@gmail.com

<sup>1</sup> L&T Ship Building, Chennai 601204, Tamilnadu, India

<sup>2</sup> School of Mechanical Engineering, Vellore Institute of Technology, Vellore 632014, Tamilnadu, India

<sup>3</sup> Siddharth Group of Engineering Institutions, Puttur 517583, Andhra Pradesh, India

electrode with the edge. A reduction in gap width increases the thickness of the layer of liquid metal (weld pool) underneath the arc, which may lead to a lack of fusion between layers. The experimental results indicate that after welding 8–10 layers, the gap may decrease by 25–40% [1]. Hence, this aspect should be considered while designing the narrow groove.

Pulsed current gas metal arc (PGMA) welding's thermal behavior affecting the weld joint characteristics has been analyzed in the shielded metal arc welding (SMAW) process. Conventional V-groove SMA butt welding, wherein the weld area and several passes are kept almost constant. In this section, significant emphasis has been placed on the welding procedure by reducing the quantity of heat transferred from the filler to the weld pool ( $Q_T$ ) and reducing the weld area with a narrow groove design. The PGMAW process has been primarily used in narrow groove welds, considering its flexibility in a metal deposition with a suitable selection of dimensionless factor ( $\phi$ ), heat input ( $\Omega$ ) and  $Q_T$  based on the bead on plate studies [5]. A narrow groove has a distinct advantage over a conventional V-groove in addition to the above. In a narrow groove, due to the low angle of attack with groove wall, the surface area exposed to arc will considerably increase compared to conventional V-groove, as shown schematically in Fig. 1. Thus, the heat density in the groove wall surface beneath the arc will dramatically reduce the thermal severity at this location.

The pulsed current arc welding (PGMAW) process's suitability in narrow gap welding has been justified by comparing its properties with narrow groove SMA welds at an almost similar area of weld deposit. However, narrow gap welding with the GMAW process has been avoided because controlled spray mode of metal deposition is achieved at a higher deposition rate leading to a comparatively severe weld thermal cycle. Further, carrying out weld deposition at a significantly low angle of attack to the

groove wall generally requires higher heat input to achieve sidewall fusion. Such a variation in GMAW can only be achieved by increasing the welding current further, much above the transition level leading to further severity of the weld thermal cycle.

## 2 Experimental Details

### 2.1 Chemical Composition of Base Metal

The chemical composition of different base metal samples was performed using spark emission optical spectroscopy with a 3-mm-diameter spot size. The test was conducted on the weld joint's transverse direction, base metal, and mechanically flattened welding electrode to accommodate the test spot. However, the CHN infrared analyzer was used to find the amount of nitrogen content in the base metal and weld. The chemical composition of 25-mm-thick extruded stainless steel pipes of AISI 304LN grade having NB of 300 mm base material is depicted in Table 1.

### 2.2 Welding Consumables

The welding consumables have been primarily divided into two categories, filler wire/electrode and shielding gas. The commercially available 99.98% purity argon gas was used as a shielding gas in the gas metal arc welding (GMAW) with a non-coated filler rod. The selection of the filler rod and welding processes was purely based on the base metal's physical and chemical composition. The base metal selection was primarily based on the amount of  $\delta$ -ferrite content (4–8%) in the weld microstructure to [6, 7] eliminate the hot cracking problem. The specification of the welding consumables used in the SMA and PGMA welding processes is given in Table 2.

### 2.3 Welding Power Source and Fixtures

The entire work was carried out with M/s ESAB make, ARISTO 2000-LUD 450 UW model, and MEK 44C wire feeder unit. The selected welding power source worked for GTAW, SMAW, GMAW, and PGMAW welding processes with synergic and non-synergic modes. The machine operated in both DC straight and reverse polarity. The power source was capable to operate with peak current ( $I_p$ ) and base current ( $I_b$ ) in steps of 4A, whereas the peak duration ( $t_p$ ) and pulse frequency ( $f$ ) could be operated in steps of 2 Hz and 0.1 ms, respectively. In order to do the pipe welding in a 1GR position, an appropriate fixture was designed and fabricated (Fig. 2). The fabricated fixture had a torch manipulator, and a flexible torch holding device supporting the rotation of the pipe. A modern torch

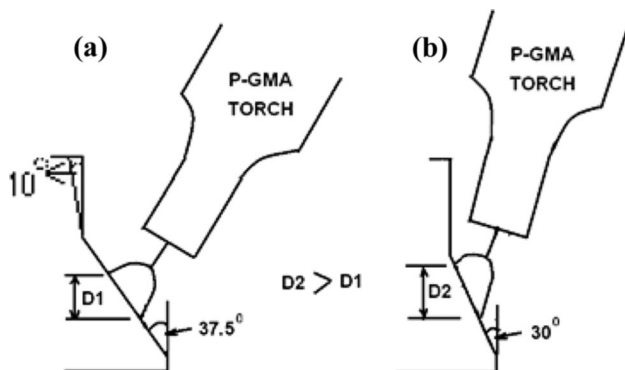


**Fig. 1** Schematic diagram showing surface area exposed to arc marked by its cross section in **a** conventional V-groove and **b** typical narrow groove design

**Table 1** Chemical composition of base metal

Type of Base metal	Source	Chemical analysis (Wt.%)									
		C	Cr	Ni	Mn	N	Mo	Si	Cu	S	P
ASS (304LN)	ASME Section IX	0.035	18–20	8–11	2.0	0.1–0.16	–	0.75	–	0.03	0.04
	Supplier test certificate	0.024	18.8	9.25	1.73	0.15	–	0.55	–	0.001	0.022
	*Laboratory test	0.023	19.02	9.14	1.82	0.16	0.19	0.57	0.30	0.002	0.021

\* Spark emission optical spectroscopy

**Table 2** Specifications of the welding consumables

Type of Process	Specification of weld consumable		
	Specification under AWS/ASME	Electrode size (mm)	Flux material (Class)
PGMAW	ER308L	1.2	–
GMAW	ER308L	1.2	–
SMAW	E 308L–15	3.15 and 4.0	Basic coated
GTAW	ER 308 L	2.0 and 2.5	–

**Fig. 2** Photograph image of the torch manipulator and pipe holding fixture

carriage with a trolley was used to position the torch for GMA and PGMA welding. However, the SMA pipe welding was carried out manually by controlling the manipulator's speed. The traveling equipment had the feature to change the welding speed in the range of 2.5–84.5 cm/min.

#### 2.4 Nozzle Design

The photograph of the newly designed narrow torch nozzle is shown in Fig. 3. The nozzle has been designed and fabricated with the following features like narrow torch nozzle having a rectangular cross section of enough depth

**Fig. 3** Photograph showing GMA narrow torch nozzle

at the gas flow outlet. The torch manipulation required for setting the optimum angle of attack in various narrow groove designs could be easily achieved. Internal cross-sectional area at the outlet of narrow torch nozzles was kept the same as that of conventional one such that gas shielding of the arc was least affected. The narrow torch nozzle's wall thickness was reduced to 1 mm by providing a proper water cooling arrangement. Moreover, the heat accumulation at the thinner wall cross section did not occur due to considerably higher arc energy and the entire torch nozzle body during the welding operation.

#### 2.5 Conventional and Narrow Weld groove

The conventional V-groove used to prepare the weld confirms the ASME Section IX of the Boiler and Pressure Vessel Code. The schematic diagram of the weld groove used to perform the SMA, PGMA pipe welding, and the

matching consumable insert with the same chemical composition of the filler is shown in Fig. 4a, b, respectively. The designing of the narrowest weld groove was approached in steps for PGMAW and SMAW processes as schematically shown in Figs. 5, 6, respectively, by keeping in view the practical difficulties of adopting the welding procedure to produce the sound weld. The welding of narrow groove pipes was also carried out in a 1GR position by following a similar procedure used in the conventional groove concerning the GTAW passes. The welding procedure was also established by asserting repeatability on at least two full pipe weld joints. However, filler passes were carried out at a much lower angle of attack to the groove wall by semi-automation mode in PGMAW and manually in SMAW processes, compared to that used in the conventional groove welding procedure. In PGMA weld joints, all the passes were carried out with a 1.2-mm-diameter filler wire using a newly developed torch nozzle device with appropriate torch manipulation in the groove, whereas, in SMA welds, the first two layers of filler passes were carried out using a 3.15-mm-diameter electrode, while the remaining layers were carried out using a 4-mm-diameter electrode.

## 2.6 Welding Processes

### 2.6.1 Pulsed Current Gas Metal Arc Welding (PGMAW)

A conventional V-groove was prepared to carry out the PGMA weld joints by changing the  $\phi$  value from 0.05 to 0.25. The work was performed with two different kinds of heat input ( $\Omega$ ) levels of  $9.2 \pm 0.35$  kJ/cm and  $7.8 \pm 0.35$  kJ/cm. At a constant heat input of  $7.8 \pm 0.5$  kJ/cm, varying  $\phi$  with values of 0.05 and 0.25 was preferred for the narrow gap PGMA welding. The pipe's transverse axial shrinkage was estimated by dividing the pipe into eight equal quadrants on the circumferential direction of the pipe. After each weld pass deposition, the variation in distance between two axial points at a known

distance was measured (Fig. 7). The heat transferred to the weld pool ( $Q_T$ ) and heat input per pass ( $\Omega$ ) was estimated by assuming the efficiency of thermal heat transfer ( $\eta_a$ ) as 0.7 [5, 8]. Finally, the weld joints characteristics were associated with the average heat input ( $\Omega$ ) per pass employed in the multiple filler pass on PGMA welding.

$$\text{Heat input (kJ/cm)} = \eta \times \frac{\text{Welding current (A)} \times \text{Arc voltage (V)}}{1000 \times \text{Welding speed (cm/s)}} \quad (1)$$

### 2.6.2 Shielded Metal Arc Welding

The conventional and narrow weld grooves were used to carry out the SMAW welding with a basic electrode of  $\phi$  3.15 mm and 4.0 mm (SFA5.4 E308L–15) at DCEP electrode polarity. The process efficiency ( $\eta$ ) on an average of 0.7 was used to calculate the SMA welding's heat input [9]. Finally, the weld joints characteristics were associated with the average heat input ( $\Omega$ ) per pass employed in the multiple filler pass on SMA welding.

## 2.7 Porosity/Inclusion Content of the Weld

An optical microscope with image analysis software was used to measure the amount of porosity and inclusion of base metal and weld deposits. The examination was done on the transverse section of the unetched weld joint. The analysis was carried out on the 21 randomly captured micrographic images under 100X magnification. The area fraction method was preferred to find the amount of porosity and inclusion content.

## 2.8 Mechanical Properties

### 2.8.1 Tensile Testing

The tensile testing specimen was prepared as per the ASTM E8M specification. Three tensile test specimens were prepared and tested to get an average of test results. The INSTRON universal testing machine was used to perform the test with a strain rate of 0.003/s. The tensile specimens were collected in the longitudinal and circumferential directions of the base metal and weld joint. The axial weld (longitudinal direction) base metal and weld metal tensile specimens were machined for a gauge length of 50 mm. All weld (circumferential direction) tensile specimens were prepared with 25 mm gauge length. The axial and all weld tensile specimens have diameters of 5 and 10 mm, respectively. The 0.2% offset strain was used to predict the yield strength of the weld.

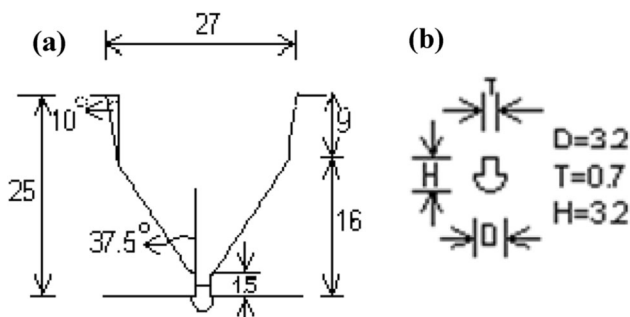


**Fig. 4** Schematic diagram of **a** V-groove 27 mm wide and **b** dimension of SMA and PGMA insert

**Fig. 5** Plain diagram of **a** narrow U-groove with 20 mm groove width, **b** narrow U-groove with 17 mm groove width, and **(c)** narrow U-groove with 15 mm groove width used for welding of pipes

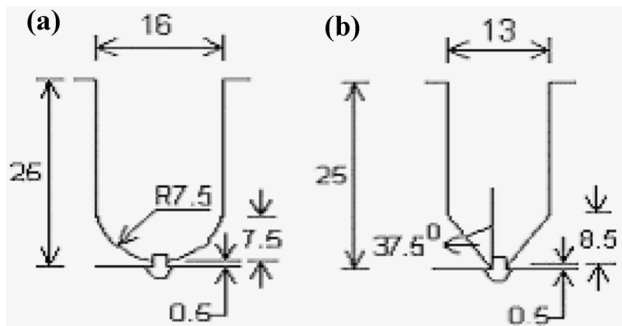
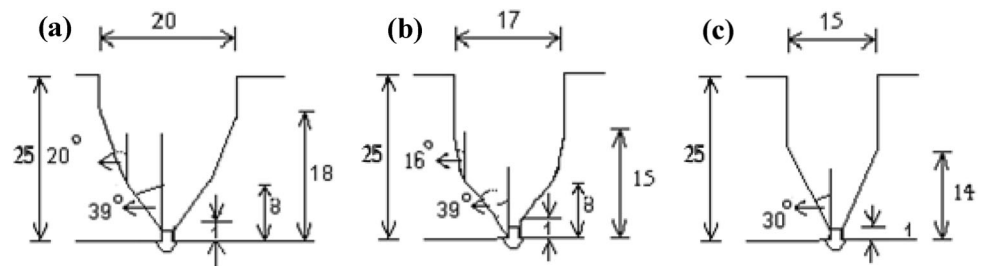


**Fig. 6** Plain diagram of **a** narrow U-groove with  $0^\circ$  bevels and 16 mm groove width and **b** narrow U-groove with  $0^\circ$  bevel and 13 mm groove width used for SMA welding of joints

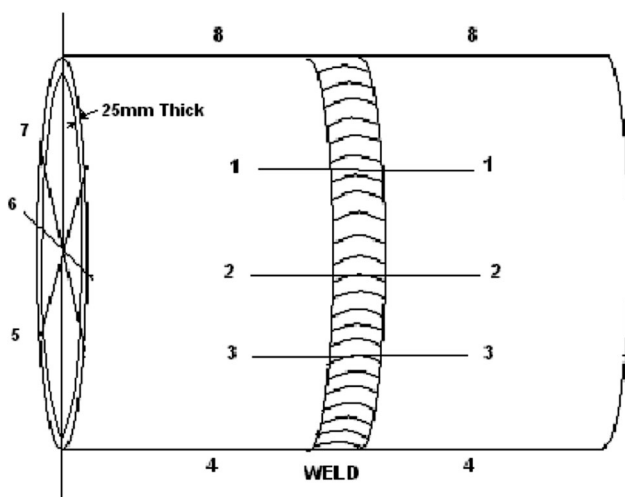


**Fig. 7** Schematic diagram showing circumferential locations at which transverse axial shrinkage was measured across two axially located points

**2.8.2 Charpy Impact Toughness Testing**

The Charpy V-notch ( $C_v$ ) impact toughness test was performed as per ASTM E23 specification. The specimen was prepared with the square cross section ( $10 \times 10$  mm) size. The notch was precisely located on the base material’s transverse and circumferential direction. However, the notch was precisely located in the circumferential direction of weld metal in order to propagate the crack along the welding direction.

**2.8.3 Hardness measurement**

The Vickers microhardness machine was used to carry out the hardness test on the base metal and weld joint. A load of 100 g was used to measure the hardness across the weld and HAZ locations. In general, minimum load is preferred to conduct the hardness test on the HAZ, which may provide slight indentation and precise results.

**2.9 Microstructure Studies**

The microstructural studies were performed on the polished specimens electrolytically etched with 10% oxalic acid solution. The specimens were cut in the transverse section of the base metal and PGMA and SMA weld metal. An optical microscope (AXIOVERT 200 MAT) was primarily used to find the microstructure on the multi-pass SMA and PGMA weld joints. The columnar or coaxial dendrite content was measured on the multi-pass weld’s microstructure. The axio vision software-based image analyzer was used to find the amount of dendrite on the weld metal. The analysis was done on the 21 randomly captured micrographic images under different magnifications.

**3 Results and Discussion**

**3.1 Weld groove Design and Size**

The macro-photographs revealed from the transverse sections of the narrow groove PGMA welds with the weld width of 17 mm, 15 mm, and 11 mm at a given  $\phi$  of 0.05 are shown in Fig. 8a, b and c, respectively. At a higher  $\phi$  (0.25), the macro-photographs of the narrow groove PGMA welds with the groove width of 15 mm and 11 mm in the transverse sections are shown in Fig. 9a, b. Likewise, the macro-photographs of the narrow groove SMA weld joints with the groove width of 14 mm and 11 mm in the transverse sections are shown in Fig. 10a, b. The summarized data of the total number of passes, average  $\Omega$  in filling passes, area of the weld deposit, and overall cumulative transverse shrinkage observed in narrow groove SMA and

**Fig. 8** Macro-photographs of narrow groove PGMA weld joints prepared with weld width of **a** 17 mm, **b** 15 mm, and **c** 11.5 mm

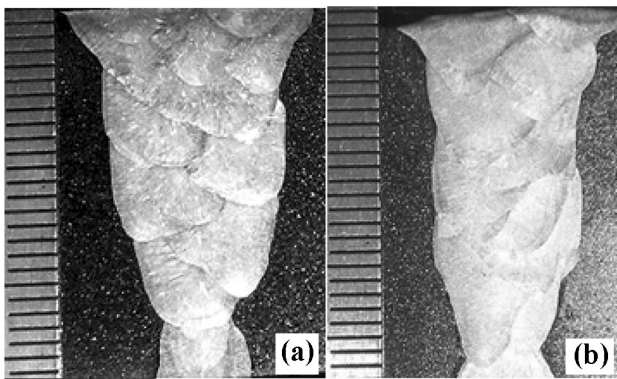
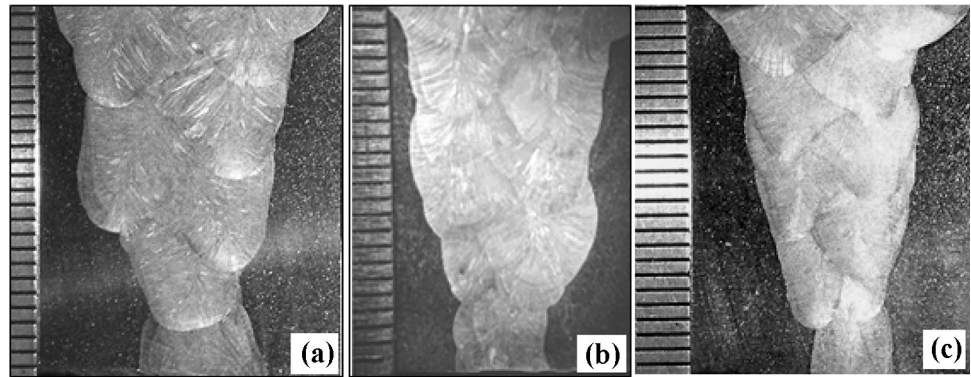


**Fig. 9** Macro-photographs show narrow groove PGMA weld joints prepared with weld width of **a** 15 mm and **c** 11.5 mm

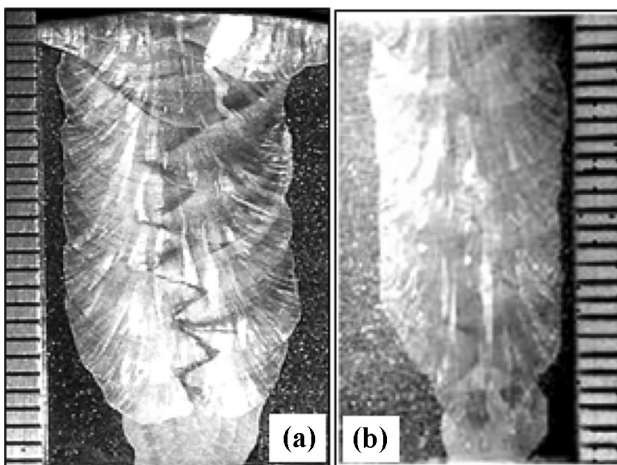


**Fig. 10** Typical macro-photographs show narrow groove SMA weld joints prepared with weld width of **a** 14 mm and **b** 11 mm

PGMA weld joints are clearly depicted in Table 3. In PGMA welds, the influence of  $\phi$  and  $Q_T$  on the above parameters is also compared in Table 3.

Figures 8, 9 and 10 show that the weld joints are basically free from lack of sidewall fusion or lack of root fusion. The characteristics of weld joints shown in Table 3 reveal that at a given area of narrow groove and  $\Omega$ , the

number of passes required in the PGMAW process has considerably reduced by 30–35% than conventionally used SMAW process. It happens due to the characteristic feature of higher deposition rate achieved [10, 11] with PGMA welding process. However, the use of narrow groove welding procedure considerably reduces the amount of weld deposition by 35–40 vol% in comparison with conventional groove weld in both PGMAW and SMAW processes.

The table further reveals that by varying welding process, cumulative shrinkage reduces by narrowing the weld groove and lowering of  $\Omega$  and  $\phi$ . It indicates a probability of a decrease in strain, particularly at the root of the narrow groove weld [4], compared to that observed in conventional V-groove pipe weld, consequently minimizing the residual stresses. The welds' radiographs depict some defects in PGMA welds, primarily as lack of fusion, while in SMA welds, the defects mainly develop as slag lines leading to lack of fusion. Table 3 shows that the semi-automated PGMA weld joints develop a relatively higher proportion of lack of fusion than manually prepared SMA weld at similar weld width. However, the lack of fusion occurs in small patches of 10–15 mm at few locations in total weld length as measured on PGMA weld radiographs except where relatively higher  $\phi$  and  $\Omega$  of 0.25 and 7.8 kJ/cm, respectively, have been used. The more considerable amount of lack of fusion at somewhat more elevated  $\phi$  and lower  $\Omega$  and  $Q_T$  (Table 3) may be attributed to comparatively lower heat introduced in the process.

In PGMA weld joints, lack of interpass and sidewall fusion at various locations primarily occur due to similar reasons observed in conventional groove weld, whereas in SMA weld joints, the slag inclusion may mainly happen due to sticking of slag on weld deposit, which becomes difficult to remove during interpass cleaning due to an increase in the magnitude of wedging effect [1], especially in case of narrow gap welding. The defects revealed have been analyzed and correspondingly marked in the pipe welds' proper location about the weld pass's starting sector (Fig. 7).

**Table 3** Summarized influence of weld data on type and the average proportion of defects discarded from narrow groove PGMA and SMA weld joints

Process	Groove width (mm)	Weld width (mm)	$\phi$	Total number of passes	Average $\Omega$ in filling passes, (kJ/cm)	Average $Q_T$ in filling passes (kJ/cm)	Area of machined groove (mm <sup>2</sup> )	Area of weld deposited (mm <sup>2</sup> )	Overall cumulative transverse shrinkage (mm)	Fractional length of LOF of the total weld (%)	Type of defects
PGMAW of fusion	20	17	0.06	12	9.4	11.4	340	267	5.0 ± 0.35	1.0	Lack
	17	15	0.05	12	7.5	11.1	300	239	4.25 ± 0.31	8.0	
			0.25	15	8.0	9.9	242	242	4.43 ± 0.40	10.2	
	15	11.5	0.05	10	7.5	11.1	270	215	4.04 ± 0.16	11.5	
0.25			11	7.9	9.9	225	225	4.20 ± 0.28	24.0		
SMAW	16	14	–	19	9.9	–	368	274	4.76 ± 0.68	5.3	Slag line and lack of fusion
	13	11	–	17	7.4	–	275	220	3.90 ± 0.37	7.0	

### 3.2 Chemical Composition and $\delta$ -Ferrite Content

The chemical compositions of the different weld joints are clearly shown in Table 4. The WRC-92 diagram was used to estimate the amount of delta ferrite content in the weld metal [6]. The table depicts that the base metal dilution can provide 0.1 wt% of nitrogen to the weld and minimize its  $\delta$ -ferrite content [6]. The filler location of PGMA weld has

4–7% of  $\delta$ -ferrite content which shows the ferrite–austenite (FA) solidification mode. In disparity to that, in SMA weld, the austenite–ferrite (AF) mode of solidification is observed with negligible  $\delta$ -ferrite (Table 4).

In the root pass carried out by the GTAW process, the  $\delta$ -ferrite is considerably higher in PGMA welds than that observed in SMA welds. It indicates that the root region gets diluted more by PGMAW filler metal having

**Table 4** Chemical composition and  $\delta$ -ferrite percentage of the narrow groove SMA and PGMA weld

Process	Weld width (mm)	$\phi$	$\Omega$ kJ/cm	Chemical analysis of weld metal (Wt.%)										
				C	Cr	Ni	Mn	N	Mo	Si	Cu	S	P	
PGMAW	17	0.06	9.4	0.025	19.10	9.37	1.63	0.10	0.16	0.48	0.19	0.01	0.009	
	15	0.05	7.5	0.029	19.08	9.35	1.56	0.10	0.14	0.46	0.20	0.012	0.007	
		0.25	8.0	0.027	18.9	9.42	1.52	0.10	0.15	0.56	0.21	0.008	0.002	
		0.05	7.5	0.024	19.2	9.64	1.61	0.10	0.15	0.56	0.20	0.009	0.002	
	0.25	7.9	0.025	19.1	9.54	1.62	0.10	0.15	0.56	0.21	0.008	0.002		
SMAW	14	–	9.9	0.029	18.45	11.1	2.34	0.10	0.05	0.50	0.12	0.006	0.013	
	11	–	7.4	0.042	18.35	11.0	2.41	0.10	0.08	0.58	0.15	0.012	0.018	
Equivalents		Estimated			$\delta$ -ferrite content (%)									
$Cr_{eq}$	$Ni_{eq}$	$\delta$ -ferrite content (%)		Solidification mode			Root passes		Filler passes					
19.26	12.29	4		FA			4.06		5.45					
19.22	12.42	4–5		FA			4.50		5.65					
19.05	12.42	6–8		FA			4.66		6.94					
19.35	12.53	4–5		FA			3.00		4.10					
19.25	12.47	4–5		FA			3.00		5.70					
18.50	14.15	3–4		AF			1.50		3.2					
18.43	14.55	2–3		AF			1.50		2.7					

comparatively higher estimated  $\delta$ -ferrite content (Table 4) in comparison with that in SMA weld. The narrow groove SMA weld in concurrence to the earlier observations on the conventional groove also shows austenite–ferrite (AF) mode of solidification, representing a significant decrease in chromium content due to the oxidation that occurs during metal transfer and the effect of base metal dilution. Table 4 further depicts that with the variation in  $\phi$  and  $\Omega$  in PGMA welds, welds' chemical composition with different groove designs has shown insignificant deviation primarily due to similar metal deposition procedures. Thus, 4–7% of  $\delta$ -ferrite content has been observed in all the welds. The narrow groove SMA weld joint with 11 mm weld width has a significantly higher carbon amount than that in the narrow groove weld joint with 14 mm weld width and conventional V-groove weld joints. However, it is observed that the carbon content of the narrow groove weld joints with 11 mm weld width is close to that of the filler metal, indicating lower dilution of base metal. The narrow groove weld which is comparatively shallow includes angle of attack with the groove wall of the order of  $25\text{--}30^\circ$ , while in narrow groove weld joint with 14 mm weld width and conventional V-groove weld joints have the angle of attack of the order of  $40\text{--}45^\circ$  and  $70\text{--}75^\circ$ , respectively. Hence, it may be due to the PGMA narrow groove welds fabricated at lower  $\Omega$  (Table 3) and 4–7%  $\delta$ -ferrite content (Table 4). The joint is primarily less prone to solidification cracking [12–14] compared to the SMA weld joint. The microstructure of delta ferrite content on PGMA and SMA welded joint with various narrow groove is typically shown in Fig. 11.

### 3.3 Mechanical Properties

#### 3.3.1 Tensile Properties

The tensile properties of the narrow groove pipe welds fabricated by using PGMA and SMA welding processes are shown in Tables 5, 6. The estimated results are taken from longitudinal (axial weld direction) and circumferential (all weld directions) directions of the weld joint. The strain hardening exponent ( $n$ ) and dimensionless material constant ( $\alpha$ ) of the tensile properties were estimated by using Ramberg–Osgood expression [1] to characterize primarily the response to fracture of the material. The typical fractography of PGMA welded 11 mm width narrow groove welds with 11 mm weld width at different  $\phi$  of 0.05 and 0.25 are compared with SMA weld is clearly depicted in Fig. 12(a–c), where the fracture has taken place from weld under the uniaxial tensile test of a longitudinal specimen of the weld joint.

Tables 5 and 6 reveal that weld deposit (circumferential direction) has comparatively higher yield strength and

elongation under uniaxial tension in the circumferential direction than those observed in the longitudinal direction of weld joints fractured from the weld. The weld metal tensile properties have been influenced by the microstructural anisotropy resulting from the orientation of coaxial morphology of dendrite in the weld deposit [15], whereas in comparison with the base metal, the yield strength ( $\sigma_y$ )-to-ultimate tensile strength ( $\sigma_u$ ) ratio of the weld significantly increases from 0.5 to 0.76 with a considerable sacrifice in elongation, resulting in a relatively higher value of strain hardening exponent ( $n$ ). Compared to SMA weld, the narrow groove PGMA welds have significantly higher tensile properties in both the longitudinal and circumferential directions. However, compared to their respective conventional groove, both PGMA and SMA narrow groove weld joints show a marginal improvement in tensile properties primarily due to the similar chemical composition of weld deposit.

The fractography of the narrow groove SMA weld of weld width of 11 mm (Fig. 12) shows considerably higher inclusion content along with fine wavy markings near the cavity, whereas narrow groove PGMA weld (11 mm weld width) of various  $\phi$  of 0.05 and 0.25 (Fig. 12), respectively, shows widespread ductile fracture behavior with fine dimples combined with significantly less porosity content (Table 10) in the SMA weld. However, both PGMA and SMA narrow groove weld joints (Fig. 12) show the considerably higher plastic flow of the austenite matrix marked by fine wavy markings near the cavity than those observed in corresponding conventional groove welds due to substantially higher refined region in the former.

#### 3.3.2 Charpy Impact Toughness

Charpy impact energy absorbed in PGMA and SMA weld joints with notch orientation in the circumferential direction is given in Table 7. It is observed from the table that all the PGMA and SMA weld joints have passed the acceptance criterion of 70 J in the as-welded state for weld metal [16]. It has been further observed that narrow groove PGMA welds have appreciably better  $C_v$ -impact toughness and lateral expansion than that observed in SMA weld joint. However, in comparison with base metal and conventional groove welds, narrow groove PGMA welds show almost equivalent  $C_v$ -impact toughness despite variation in  $\phi$ .

The weld metal impact toughness primarily depends on chemical composition, porosity content, and microstructure refinement [15]. The chemical composition of filler metal used in PGMA welds has a significantly higher Mn/C ratio and considerable nickel content than that used in SMA weld. Further, PGMA welds have significantly lower porosity content (Table 10) than that observed in SMA



**Fig. 11** Microstructure of delta ferrite for various weld metal deposits **a** 17 mm width PGMA weld, **b** 15 mm width PGMA weld, **c** 11.5 mm width PGMA weld, d) 14 mm width SMA weld

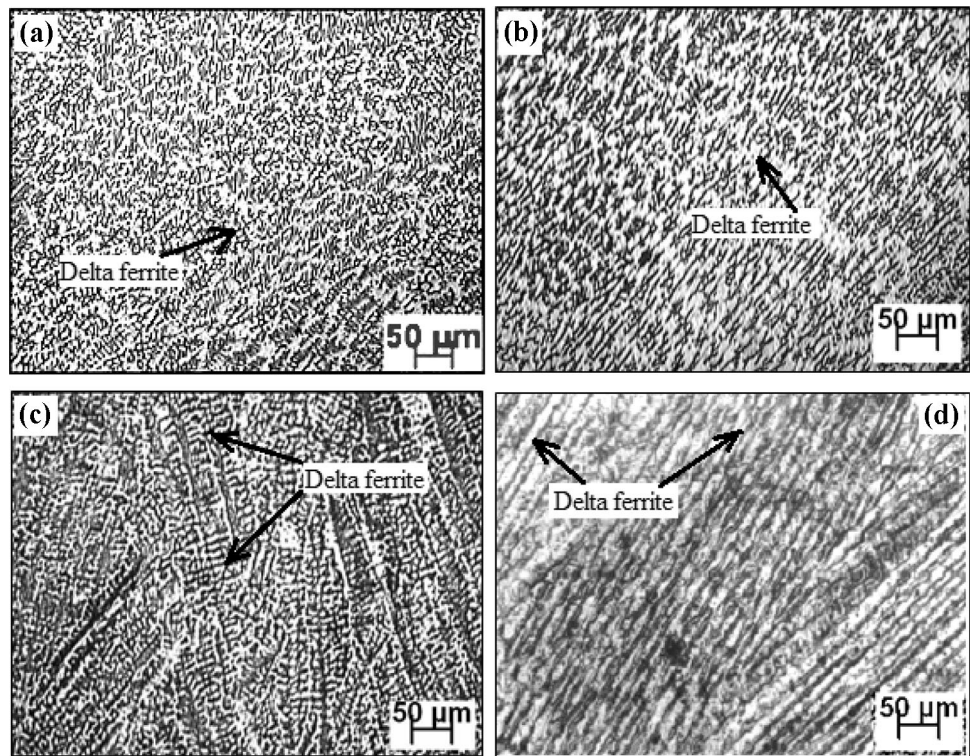


**Table 5** Tensile properties in the longitudinal (axial) direction of narrow groove weld joints

Process	Weld width (mm)	φ	Ω kJ/cm	Tensile properties								Failure region				
				UTS (MPa)	YS (MPa)	YS/UTS Ratio	Elongation(%)	n	α							
PGMAW	17	0.15	9.4	653	372		48.1	5.80	24.26							
				653	653	365	363	0.56	44.6	45.8	5.67	5.70	22.71	22.91	Weld	
				652	352		44.7	5.64	21.75							
	15	0.05	7.5	649	654	372	368	0.56	46.7	45.0	5.80	5.82	22.64	21.54		
				653	369		46.0	5.81	21.53							
				660	363		44.3	5.84	20.46							
				0.25	8.0	635	633	354	344	0.54	45.8	43.8	5.14	5.50	27.53	22.73
				634	342		42.8	5.51	21.73							
				630	336		42.8	5.85	18.93							
	11.5	0.05	7.5	646	651	366	364	0.56	43.7	45.8	5.80	5.70	24.26	22.91		
				650	363		45.6	5.67	22.71							
				657	362		48.0	5.64	21.75							
0.25				7.9	637	631	348	344	0.55	31	34.7	6.32	6.28	21.94	22.27	
632				346		34.6	6.28	22.05								
624				339		38.4	6.24	22.81								
SMAW	14	-	9.9	560	556	358	350	0.63	22.0	22.8	6.20	6.25	20.38	20.54	Weld	
				554	348		21.8	6.24	20.45							
				554	344		24.6	6.31	20.79							
	11	-	7.4	576	582	362	354	0.61	21.9	23.4	6.14	5.92	20.34	21.26		
				578	354		22.5	5.88	20.33							
				592	347		25.8	5.74	22.11							

**Table 6** Tensile properties in circumferential (all weld) direction of narrow groove weld joints

Process	Weld width (mm)	$\Phi$	$\Omega$ kJ/cm	Tensile properties										
				UTS (MPa)		YS (MPa)		YS/UTS Ratio	Elongation (%)		n		$\alpha$	
PGMAW	17	0.15	9.4	628	616	476	466	0.76	39.9	40.0	6.04	6.10	26.76	29.01
				614		465			40.0		6.09		28.99	
				606		456			40.0		6.16		31.29	
	15	0.05	7.5	623	622	468	461	0.74	39.9	40.5	7.19	6.86	30.40	38.42
				622		459			40.4		6.84		38.62	
				620		456			41.2		6.54		46.24	
				626	618	475	466	0.75	43.0	40.4	7.92	7.43	32.63	33.44
				617		464			39.4		7.23		33.05	
				611		459			38.8		7.14		34.64	
	11.5	0.05	7.5	667	668	419	414	0.62	56.6	53.6	8.32	7.86	28.74	31.3
				668		413			55.4		7.92		31.84	
				669		411			48.9		7.33		33.36	
				624	641	439	426	0.66	30.9	31.7	6.24	6.39	39.48	36.01
				641		425			31.1		6.42		35.34	
				657		414			33.1		6.51		33.23	
SMAW	14	-	9.9	598	580	434	446	0.78	32.2	28.1	8.39	7.56	26.62	23.2
				577		448			27.9		7.53		23.10	
				566		455			24.2		6.76		19.88	
	11	-	7.4	593	598	425	431	0.72	44.0	39.7	6.38	6.45	38.84	35.13
				599		432			39.0		6.45		34.43	
				602		435			36.0		6.53		32.13	

Note:—n and  $\alpha$  are strain hardening exponent and dimensionless material constant as given in Ramberg–Osgood expression [1]

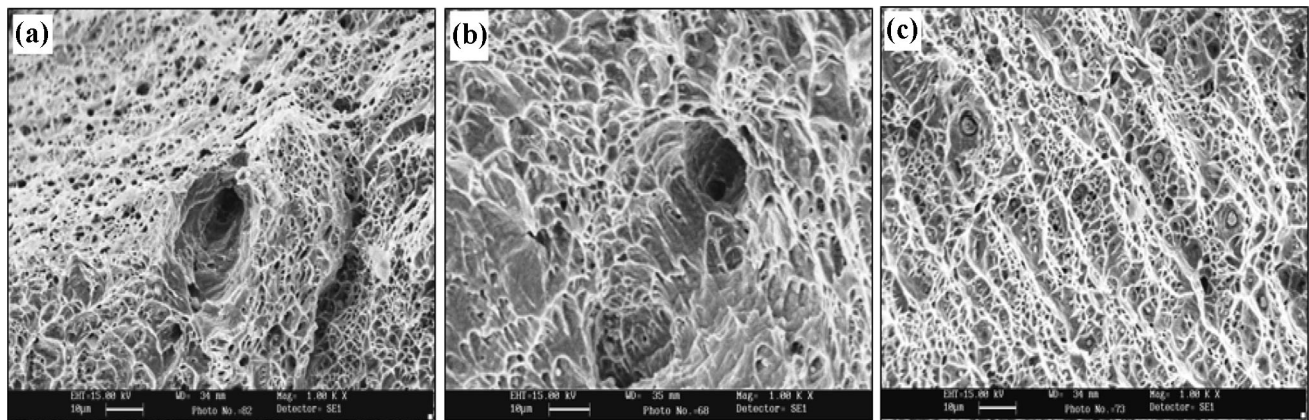


**Fig. 12** At a given  $\Omega$  of around 7.7 kJ/cm and weld width of 11 mm, typical SEM photographs of fractured surface in axial tensile specimens observed in narrow groove PGMA welds at different  $\phi$  of **a** 0.05, **b** 0.25, and **c** SMA weld

weld. PGMA welds also have considerably higher refined dendritic microstructure (Table 8) especially with the lowering of  $\phi$  in comparison with SMA weld joints at a given  $\Omega$ . Thus, despite higher  $\delta$ -ferrite content, which

generally tends to decrease the toughness, these various positive aspects may have primarily contributed to comparatively higher impact properties in PGMA welds than those observed in SMA weld joints.

**Table 7** Charpy impact toughness of narrow groove PGMA and SMA weld joints

process	Weld width (mm)	$\phi$	$\Omega$ kJ/cm	Charpy impact properties					
				Energy absorbed, (J)		Lateral expansion, (mm)			
PGMAW	17	0.06	9.4	136	132	2.66	2.59		
				133		2.61			
				127		2.50			
	15	0.05	7.5	133	132	2.61	2.59		
				132		2.59			
				131		2.57			
				131		128		2.64	2.60
				128				2.62	
				125				2.54	
	11.5	0.05	7.5	137	134	2.67	2.63		
				135		2.64			
				129		2.59			
128				126		2.54		2.50	
126						2.51			
124						2.46			
SMAW	14	-	9.9	97	94	1.84	1.78		
				94		1.78			
				91		1.72			
	11	-	7.4	88	91	1.44	2.47		
				92		1.53			
				93		1.65			

**Table 8** Area fraction refinement of dendrite in narrow groove PGMA and SMA weld

Process	Weld width (mm)	$\phi$	$\Omega$ kJ/cm	Coaxial dendritic region (%)	Refined region (%)
PGMAW	17	0.06	9.4	36.3	63.7
	15	0.05	7.5	25.4	74.6
		0.25	8.0	31.8	68.2
		11.5	0.05	7.5	18.8
		0.25	7.9	25.7	76.3
SMAW	14	-	9.9	56.1	43.9
	11		7.4	69.6	30.4

### 3.3.3 Hardness

At a given weld width of 14–15 mm, the estimated hardness value across the narrow groove PGMA and SMA weld joints is shown in Fig. 13. Similarly, at a given weld width of 11 mm, the hardness distribution across PGMA and SMA weld joints is compared in Fig. 14. At a given weld width of 14 mm and 11 mm, the hardness distribution in weld deposit and HAZ of both PGMA and SMA weld joints is similar across the region. It is further observed that both PGMA and SMA welds with 11 mm weld width have

a marginally lower hardness than those observed in corresponding welds with 14 mm width. However, at minimum heat input ( $7.7 \pm 0.35$  kJ/cm), the influence of  $\phi$  on hardness distribution appears to be practically negligible in the weld and HAZ of both conventional and narrow groove PGMA weld joints. However, compared to conventional groove SMA weld, relatively higher hardness distribution in the weld region and considerable scattering across the weld and HAZ region are observed in narrow groove SMA weld joints.

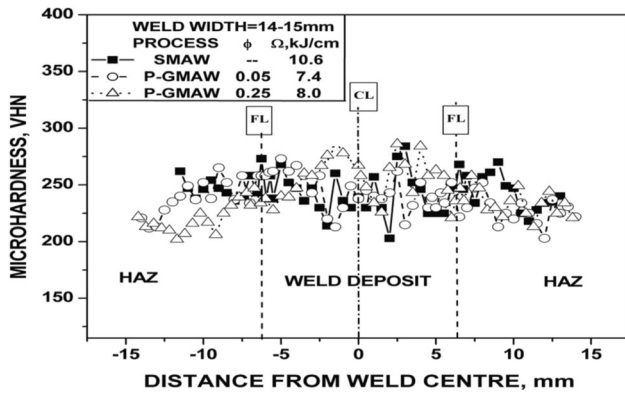


**Fig. 13** At a given weld width of 14 mm, the narrow groove PGMA and SMA welds' hardness value with variation  $\phi$  and  $\Omega$

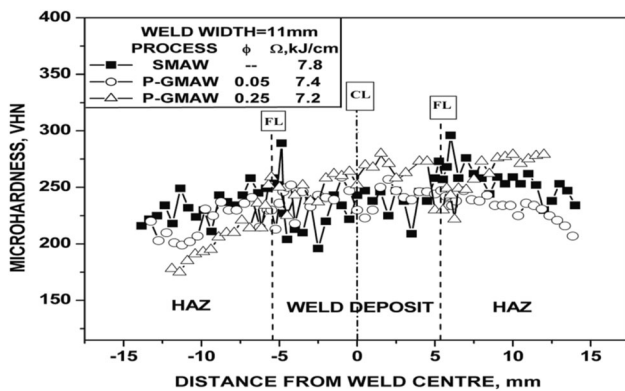


**Fig. 14** At a given weld width of 11 mm, hardness value of the narrow groove PGMA and SMA welds with the variation in  $\phi$  and  $\Omega$

PGMA welds are comparatively less scattered in hardness across the weld and HAZ at both the  $\Omega$  and  $\phi$  levels. It indicates uniformity in microstructure due to the considerable scale refinement of the dendritic microstructure observed in conventional groove welds. Simultaneously, a significant amount of scattering in hardness may have occurred due to the presence of a comparatively more amount of various kinds of regions of the microstructure having coaxial dendrite and refined dendritic region (Table 8) in the SMA weld deposit.

### 3.4 Microstructure

The heat dissipation into the solid metal primarily controls the crystallization of metal during welding, and some amount of heat is comparatively being dissipated into the atmosphere. The effect of heat transfer influences the type of grain, grain size, and orientation of the weld and HAZ grains [16–18]. The influence of thermal behavior in the PGMA weld and the microstructural studies in narrow groove welds are compared with SMA weld deposition. At a given  $\Omega$  ( $7.7 \pm 0.35$  kJ/cm) and weld width (14 mm), the

effect of variation in  $\phi$  (0.06 to 0.25) on the PGMA weld microstructures is shown in Fig. 15a, b. Similarly, at a given  $\Omega$  ( $7.7 \pm 0.35$  kJ/cm) and weld width (11 mm), the microstructures observed at variation in  $\phi$  (0.05 and 0.25) are compared in Fig. 16a, b. The specific microstructures observed in narrow groove SMA welds deposited with a weld width of 14 mm and 11 mm are shown in Fig. 17a, b, respectively.

The microstructures presented in Figs. 15, 16 primarily depict that the narrow groove welds of both PGMA and SMA processes show similar multi-pass weld deposition features as those observed in corresponding conventional groove welds. However, the narrow groove PGMA weld deposit offers more refinement of microstructure and scarcely distributed coaxial dendritic structure with the lowering from 0.25 to 0.05 compared to that observed in conventional groove PGMA welds. The considerable refinement of microstructure has been observed to reduce  $\phi$  (0.05). It may have primarily happened due to changes in thermal shock at the time of solidification, which disrupts weld metal deposition. This effect has mainly happened due to the pulse parameters combined with less severity of weld thermal cycle in the narrow groove multi-pass weld deposition.

Compared to conventional groove weld, the narrow groove SMA welds show further increase in reheat refined regions with the reduction in weld width from 14 to 11 mm. It may be attributed primarily to a comparatively higher fraction of the interface region resulting in the subsequent multi-pass passes. The severity of the weld thermal cycle may produce partial reheat refine region at the coaxial dendrite zone. The weld metal microstructure difference has been further analyzed by the amount and distribution of coaxial dendritic and refined regions in SMA and PGMA weld metal deposits. In connection with the above statement, the table depicts that the influence of PGMAW primarily decreases the amount of coaxial dendritic region in the welds deposit compared to SMA welds.

At a given  $\Omega$  of  $7.7 \pm 0.35$  kJ/cm, the influence of practically narrowest PGMA weld on the weld HAZ microstructures at varying  $\phi$  (0.05 and 0.25) is compared in Fig. 18a, b. The HAZ microstructures near the fusion line on the narrow groove (14 mm and 11 mm) of SMA welds are shown in Fig. 19a, b. The narrow groove PGMA and SMA welded HAZ microstructure near the fusion line (Figs. 18, 19) delivers that a certain extent of coarsening of grain is observed in the case of their conventional groove welds. The HAZ grain size has been compared for various PGMA and SMA weld joints in Table 9. The table depicts that the narrow groove PGMA and SMA weld joints have comparatively less coarsening of grain than conventional groove weld. The table further reveals that narrow gap

**Fig. 15** Typical microstructures observed in narrow groove PGMA weld (14 mm weld width) joint at varying  $\phi$  of **a** 0.06 and **b** 0.25

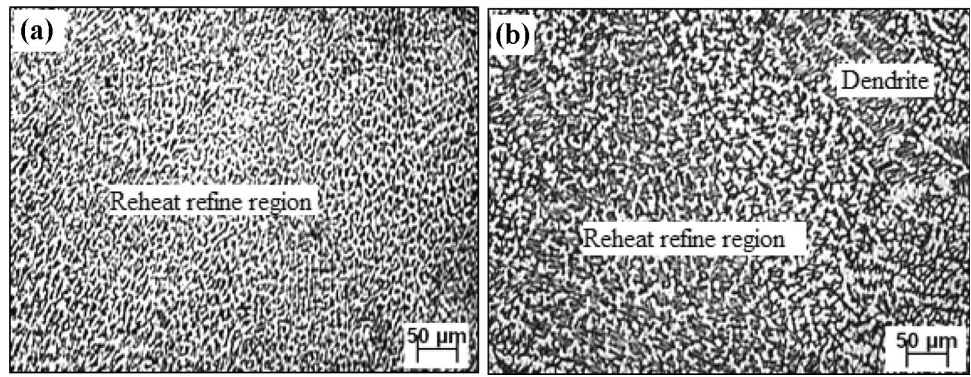


**Fig. 16** Typical microstructures observed in the PGMA weld (11 mm weld width) joint at varying  $\phi$  of **a** 0.05 and **b** 0.25

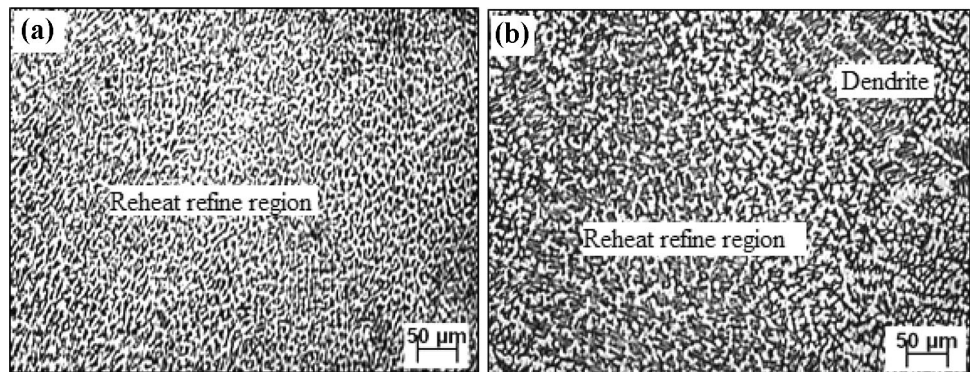


**Fig. 17** Microstructures of narrow groove SMA weld deposit prepared with **a** 14 mm and **b** 11 mm weld width

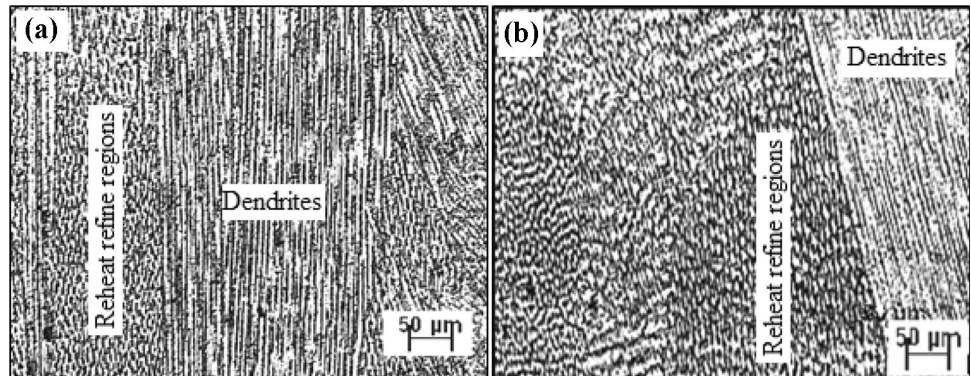


**Fig. 18** Typical microstructures of HAZ near fusion line in narrow groove PGMA weld with 11 mm weld width; **a**  $\phi = 0.05$  and **b**  $\phi = 0.25$

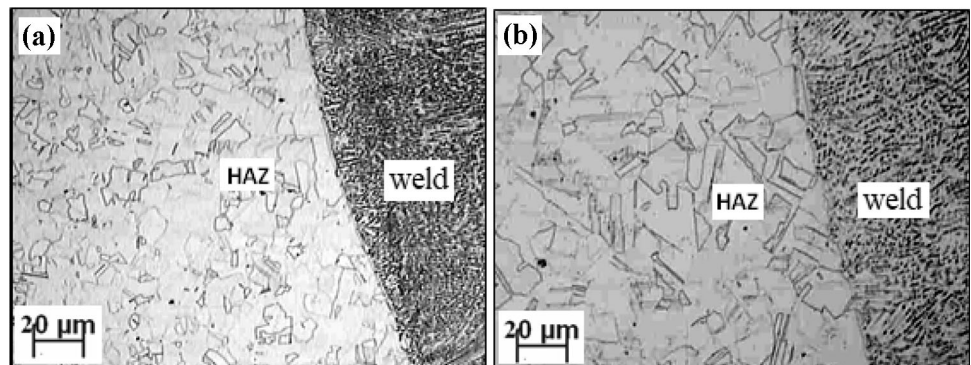


**Fig. 19** HAZ microstructure adjacent to fusion line of narrow groove SMA welds at a weld width of **a** 14 mm and **b** 11 mm

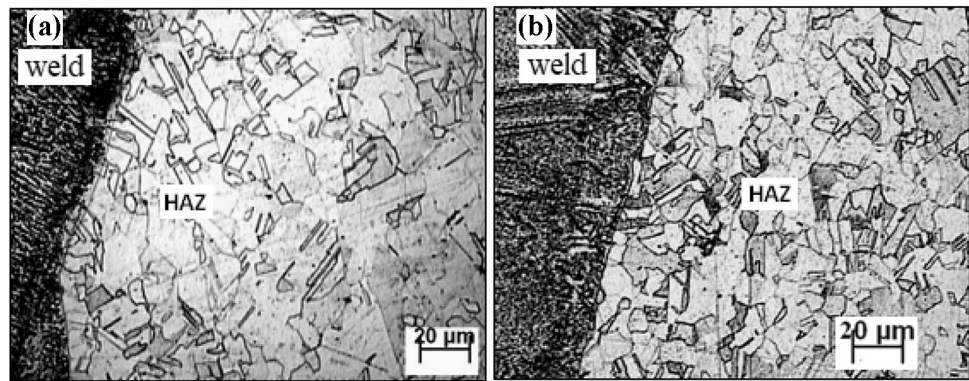


**Table 9** Grain size measurement near HAZ region at various weld joints

Process	Weld width (mm)	$\phi$	$\Omega$ kJ/cm	Avg. Grain dia. $\pm$ S.D ( $\mu\text{m}$ )			ASTM No		
				A	B	Avg. of A and B	A	B	Avg. of A and B
PGMAW	17	0.06	9.4	$16 \pm 5$	$20 \pm 4$	$17 \pm 5$	9.5	8.5	9.0
	15	0.05	7.5	$13 \pm 7$	$13 \pm 4$	$13 \pm 5$	9.5	9.5	9.5
		0.25	8.0	$13 \pm 4$	$13 \pm 2$	$13 \pm 3$	9.5	9.5	9.5
		0.05	7.5	$12 \pm 5$	$12 \pm 4$	$12 \pm 5$	9.5	9.5	9.5
	0.25	7.9	$13 \pm 3$	$12 \pm 4$	$13 \pm 3$	9.5	9.5	9.5	
SMAW	14	-	9.9	$20 \pm 3$	$20 \pm 3$	$20 \pm 3$	8.5	8.5	8.5
	11		7.4	$17 \pm 2$	$18 \pm 2$	$18 \pm 2$	9.0	9.0	9.0

S.D. is standard deviation. A and B are on either side of the weld joint

PGMA weld joints have a considerable reduction in grain coarsening than in the narrow gap SMA weld joints. It indicates that grain coarsening reduces with the change in the welding process and procedure due to a considerable decrease in weld thermal cycle severity, rising the weld deposition heat near the groove wall. However, at a given  $\Omega$  of PGMA welds, the increase in  $\phi$  from 0.05 to 0.25 marginally coarsens the grain size adjacent to the fusion line in HAZ. Such an advantage of lower  $\phi$  at a given  $\Omega$  may be beneficial to improve HAZ resistance to susceptibility to stress corrosion cracking susceptibility of HAZ in narrow groove PGMA welds compared to that in SMA weld joints.

### 3.4.1 Porosity and Inclusion Content

The amount of porosity and inclusion content in the narrow groove PGMA and SMA weld is revealed in Table 10. The inclusions on the fractured surface in the narrow groove (11 mm) PGMA and SMA welds are shown in Fig. 20b. The negligible presence of round facets in the fractography presented in Fig. 20a than those observed in 20(b) reveals that the PGMA welds have significantly less porosity content than SMA welds. The table further depicts that the

narrow groove PGMA weld joints prepared under a comparatively cleaner environment of argon gas shielding have 80–90% lower porosity or inclusion content than that of the narrow groove SMA weld joints. However, compared to conventional groove welds, PGMA welds have shown a marginal increment in porosity content.

In contrast, the narrow groove SMA welds' inclusion and porosity content have increased by almost 30%. In PGMA welds, at a given  $\phi$  and  $\Omega$ , the difference in the PGMA weld's porosity has been found similar to conventional groove welds, primarily due to insignificant difference in the pulse parameters used for weld joint. The inclusion content of SMA welds increases with the reduction in weld width primarily due to the significantly impaired detachability of slag as marked by embedded inclusions (Fig. 20) in the matrix. It has primarily happened due to the increase in strength of the thick slag layer formed at the approaching edges of the weld groove depending upon cooling conditions provided by the narrow groove [1]. The optical image of inclusion content in the as-welded narrow gap SMA weld with 11 mm width and narrow gap PGMA weld with 11.5 mm width is typically shown in Fig. 21.

**Table 10** Porosity and inclusion percentage of PGMA and SMA weld joints

Process	Weld width (mm)	$\phi$	$\Omega$ kJ/cm	Inclusions rating		Inclusion and porosity content, (Vol. %)
				Category	Severity level	
PGMAW	17	0.15	9.2	D thin/D thick	3.0–4.5	0.32
		0.05	7.4	D thin/D thick	3.0–4.5	0.19
	11.5	0.25	8.0	B thin/B thick	1.0–2.0	0.56
		0.05	7.4	D thin/D thick	3.0–4.5	0.23
				B thin/B thick	1.0–2.5	
		0.25	7.2	B thin/B thick	1.0–3.0	0.68
D thin/D thick	2.5–5.0					
SMAW	14	–	10.6	B thin/B thick	0.5–1.5	2.62
				C thick	1.0–2.5	
				D thin/D thick	2.5–5.0	
	11	–	7.8	B thin/B thick	0.5–1.5	3.19
				C thick	1.0–4.0	
				D thin/D thick	2.5–5.0	

**Fig. 20** The presence of porosity and embedded inclusions inside the narrow groove's fractography **a** PGMA weld with 11.5 mm width and **b** SMA welds of 11 mm weld width

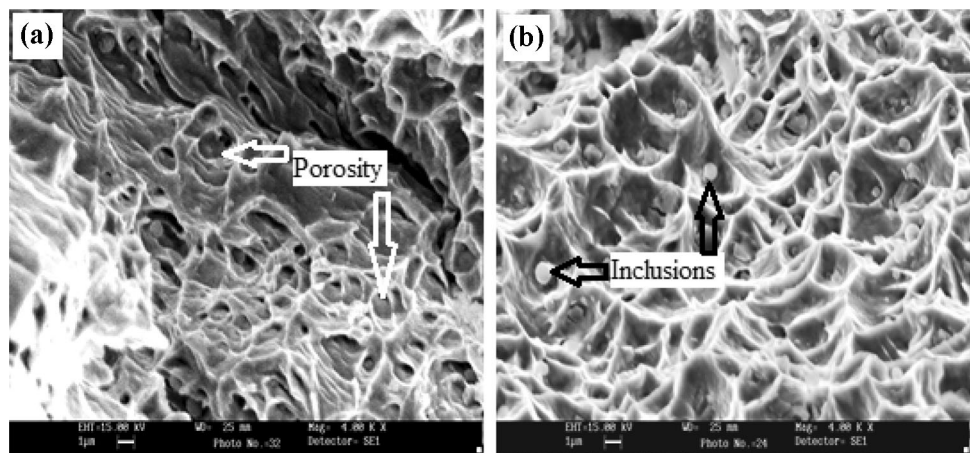
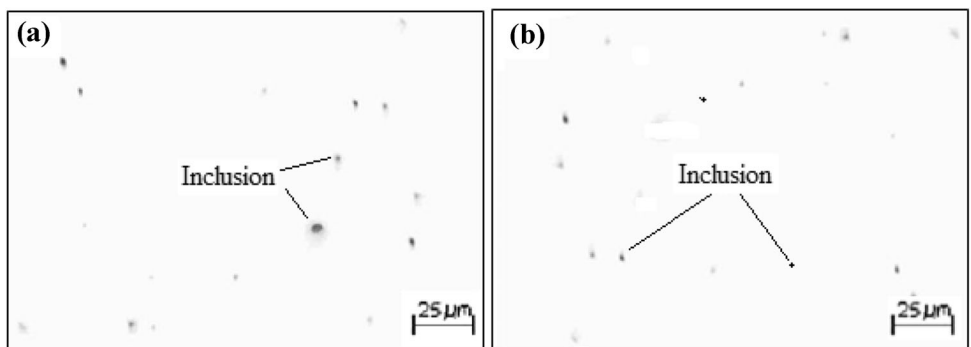


**Fig. 21** Typical presence of inclusions observed in narrow groove **a** SMA weld with 11 mm width **b** PGMA weld with 11.5 width



## 4 Conclusion

- The area of weld deposit in narrow groove joint considerably is minimized by about 35–40 vol % compared to conventional groove joint.
- The argon shielded PGMA welds have 80–90% less inclusion content than their SMA weld counterparts.
- The control of pulse parameters has considerably reduced the number of weld passes and, hence, the weld thermal cycle's cumulative effect.
- The ultimate strength (633 MPa) and yield strength (344 MPa) in the longitudinal (axial) direction of the narrow groove (11.5 mm) PGMA weld show comparatively higher values than that of narrow groove (11 mm) SMA weld.
- It is observed that both PGMA and SMA welds with 11 mm weld width have a marginally lower hardness than those observed in corresponding welds with 14 mm width.
- The narrow groove PGMA welds have appreciably better toughness (136 J) and lateral expansion (2.59 mm) than the SMA weld joint.

## References

- [1] Shtrikman, M.M. and Grinin, V.V., The automatic narrow gap welding of high strength steels and titanium alloys, *Welding Production*, 1977, 24(1), 19–23.
- [2] Swada, S., Hori, K., Kawahara, M., Takao, M. and Asano, I., Application of narrow gap process *Welding Journal*, 1979, 59(9), 17–25.
- [3] Vornovitskii, L.V., Gelpern, S.A., Tureshskii, A.V., The manual narrow gap arc welding of non-rotating joints in pipelines, *Welding Production*, 1977, 24(6), 18–20.
- [4] Murugan, S., Rai, S.K., Kumar, P.V., Jayakumar, J., Baldev Raj, and Bose, M.S.C., Temperature distribution and residual stresses due to multipass welding in type 304 stainless steel and low carbon steel weld pads, *Int. J. Pres. Ves. Pip*, 2001, 78(4), 307–317.
- [5] Rajamurugan, G., Ghosh, P.K., Prabu, K. et al. Thermal and weld bead characteristics of bead-on-plate PGMA welding of dissimilar ASS bead on HSLA Plate. *Trans Indian Inst Met*. 2020, 74, 89–106. <https://doi.org/10.1007/s12666-020-02106-4>.
- [6] Siewert, T.A., McCowan, C.N. and Olson, D.L., Ferrite number prediction to 100 FN in stainless steel weld metal, *Welding Journal*, 1988, 67(1), 289s–298s
- [7] Shankar, V., Gill, T.P.S., Mannan, S.L. and Sundaresan, S., Solidification cracking in austenitic stainless steel welds, *Sadhana*, 2003b, 28(3/4), 359–382.
- [8] Joseph, A., Harwig, D., Farson, D. F. and Richardson, R., Measurement and calculation of arc power and heat transfer efficiency in pulsed gas metal arc welding, *Science and Technology of Welding and Joining*, 2003, 8(6), 400–406.
- [9] Ghosh, P.K. and Sharma, V., Weld bead chemistry and its characteristics in pulsed MIG welded Al-Zn-Mg alloy, *Materials Transactions JIM*, 1991, 32(2), 145–150.
- [10] Suban, M., Tusek, J. and Uran, M., Use of hydrogen in welding engineering in former times and today, *Journal of Material Processing Technology*, 2001, 119, 193–198.
- [11] Govindasamy, R., “Comparative studies on conventional groove SMA and GMA welds of dissimilar 304LN ASS and HSLA steels,” SAE Technical Paper 2020-28-0405, 2020. <https://doi.org/10.4271/2020-28-0405>.
- [12] Koseki, T. and Flemings, M.C., Solidification of undercooled Fe–Cr–Ni alloys part II – microstructural evolution, *Met.Mat.-Tran A*, 1996, 27A, 3226–3240.
- [13] Lippold, J.C. and Savage, W.F., Solidification of austenitic stainless steel weldments-Part III. The effect of solidification behaviour on hot cracking susceptibility, *Welding Journal*, 1986, 62, 204s–209s.
- [14] Rajamurugan, G., Ghosh, P.K., Prabu, K. et al. Dendrite Morphological Analysis on SMA, GMA, and PGMA Welding of Dissimilar 304LN Austenitic Stainless Steel and Microalloyed Steel. *Trans Indian Inst Met*. 2020, 73, 595–611. <https://doi.org/10.1007/s12666-020-01871-6>.
- [15] Tavassoli, A.A., Assessment of austenitic stainless steels, *Fusion Engineering and Design*, 1995, 29, 371–390.
- [16] Folkhard, E., *Welding Metallurgy of Stainless Steels*, Springer-Verlag, Wien 1984.
- [17] Padilha, A. F. and Rios, P.R., Decomposition of austenite in austenitic stainless steels, *ISIJ International*, 2002, 42(4), 325–337.
- [18] Rajamurugan, G., Dinesh, D. and Ramakrishnan, A., Comparative study on grain size and HAZ width of GMA and PGMA welds of dissimilar ASS and HSLA steelplates. *Int J Mech Prod Eng Res Dev* 2018, 8, 1641–1649.

**Publisher's Note** Springer Nature remains neutral with regard to jurisdictional claims in published maps and institutional affiliations.